

See discussions, stats, and author profiles for this publication at: <https://www.researchgate.net/publication/372072777>

# Numerical simulation of local scour around the pier with and without airfoil collar (AFC) using FLOW-3D

Article in *Environmental Fluid Mechanics* · July 2023

DOI: 10.1007/s10652-023-09932-2

CITATIONS

18

READS

507

3 authors:



Lav Kumar Gupta

National Institute of Technology, Warangal

8 PUBLICATIONS 115 CITATIONS

SEE PROFILE



Manish Pandey

National Institute of Technology, Warangal

80 PUBLICATIONS 1,595 CITATIONS

SEE PROFILE



P. ANAND Raj

National Institute of Technology, Warangal

43 PUBLICATIONS 824 CITATIONS

SEE PROFILE



# Numerical simulation of local scour around the pier with and without airfoil collar (AFC) using FLOW-3D

Lav Kumar Gupta<sup>1</sup> · Manish Pandey<sup>1</sup> · P. Anand Raj<sup>1</sup>

Received: 3 February 2023 / Accepted: 11 June 2023  
© The Author(s), under exclusive licence to Springer Nature B.V. 2023

## Abstract

This paper studies the pier with Air-Foil Collar (AFC) and its effect on local scour. Simulation is carried out with two collars having diameters of  $2b$  and  $3b$ , where  $b$  is pier diameter, designated as  $d_{c1}$  and  $d_{c2}$  respectively using FLOW-3D. A total of six simulations are carried out; pier without AFC, pier with collar  $d_{c1}$ ,  $d_{c2}$  and  $d_{c1}$  in reverse to the flow direction on the sediment bed and pier with  $d_{c1}$  and  $d_{c2}$  at  $y/2$  above the sediment bed. The turbulence model used in the study is Large Eddy Simulation (LES), and the bed-load transport model utilized is van Rijn. A nested mesh configuration is used with 12.234 million mesh cells. The error between the experimental and simulated results is 7%, indicating a good correlation between them. Temporal variation of scour depth and the percentage reduction of scour depth using the AFC are explored. The percentage reduction of scour depth ( $\eta$ ) for various case studies and different orientations of the collar ranges between 11 to 100%. Scour depth contours, longitudinal scour hole profiles, transverse scour hole profiles, and streamlines are developed and analyzed for salient features.

**Keywords** Air-foil collar · Local scour · Scour depth · Large eddy simulation · FLOW-3D

## 1 Introduction

Deposition and erosion of sediment bed is a natural and complex phenomenon in the alluvial channel, which causes the change in the direction of river flow [1–3]. When the direction of river flow changes, it carries dangerous and unwanted debris which can destroy any society's sustenance [4]. Nowadays, flooding of the river is more common due to climate change which causes damage to hydraulic structures like bridge elements, abutments, caissons etc.[4–9]. Therefore, flooding of the river is a natural hazard [9–12]. The

---

✉ Lav Kumar Gupta  
gk701902@student.nitw.ac.in; lkuptace@gmail.com

Manish Pandey  
mpandey@nitw.ac.in; manishpandey3aug@gmail.com

P. Anand Raj  
anand@nitw.ac.in

<sup>1</sup> Department of Civil Engineering, National Institute of Technology Warangal, Warangal 506004, India

characteristics of natural hazards and sediment transport depend upon the change in the river flow direction [11]. The river flow capacity is affected by the change in bed elevation, i.e., erosion and deposition [13, 14]. The erosion and deposition of bed materials occur due to the action of running water, known as scouring [5, 15, 16]. Scouring around the hydraulic structure is a global problem. It is of three types, i.e., natural, contraction and local scour. Local scour occurs by destruction in the flow, resulting from downflow and horseshoe vortex [8, 16–21].

The construction of bridges has always been a complex and challenging process, especially when spanning over water bodies [22]. In some instances, it becomes necessary to place piers within the water to span long distances, which can be problematic since the foundations can be undermined, jeopardizing the structural safety of the bridge. As a result, it poses a significant concern for public safety and infrastructure, given that scouring has been responsible for 60% of bridge failures in the United States [22, 23]. For instance, in 1994, tropical storm Alberto made landfall in Georgia, USA, and caused damage to over 500 bridges due to scour. Out of these, 31 were considered unsafe and needed reconstruction because scouring reached depths between 4 and 6 m [23]. The widespread nature of scouring is evident, and it has caused significant damage through various incidents [24].

With the advancement in computer science, Computational Fluid Dynamics (CFD) became an essential tool for analyzing and visualizing the scouring process [25]. It gives significant and reliable results compared to experimental results. Nowadays, CFD is more accessible than experimental work because of difficulties like data collection, scale issues, time restriction, human error and human resources in experimental work [26]. Experimental results are obtained only where the gauges and sensors are fixed. Also, during the pandemic and health emergency, it is almost inaccessible to conduct experiments, whereas CFD becomes useful [27]. The three main turbulence models used in CFD are Reynolds-Averaged Navier–Stokes (RANS), Large Eddy Simulation (LES), and Direct Numerical Simulation (DNS) [28]. RANS solves steady-state Navier–Stokes equations, which include time-averaged velocity. It does not consider the fluctuating components, unsteadiness and anisotropic turbulence on sediment transport [29].

In turbulent flow, energy is transferred from larger scales of motion to smaller scales of motion through a process called energy cascade. The large-scale flow structures, which are characterized by their long time and length scales, dominate the momentum and energy transport. However, at smaller scales, the flow becomes more chaotic and turbulent, with small-scale eddies and vortices appearing and dissipating rapidly. In Large Eddy Simulation (LES), the goal is to simulate the large-scale flow structures accurately while modelling the smaller-scale eddies [29–32]. This is achieved by filtering out the small-scale turbulent fluctuations using a filter function and then applying a turbulence model to the remaining large-scale flow structures. The subgrid-scale turbulent fluctuations are modelled using various approaches, such as eddy viscosity models or dynamic models [25]. Chen et al. [33] investigated the effects of collar width and hook height on scour reduction through laboratory experiments and numerical simulations using FLOW-3D. They used a single hook for the laboratory experiments and a double hook for the simulations, both with collar widths of  $1.25b$  and a hook height of  $0.25b$ , where  $b$  is the pier diameter. The results showed that the pier with a single hooked collar placed on the bed reduced scouring by 42%, while the pier with a double hooked collar placed on the bed reduced scouring by 50%. Qi et al. [25] investigated the effect on local scour around an isolated pier under clear water conditions due to the tilted anticlockwise circular collar. FLOW-3D was utilized to simulate the six different cases, i.e., collar tilted on the bed at  $0^\circ$ ,  $5^\circ$ ,  $10^\circ$ ,  $15^\circ$  and  $20^\circ$ . It was concluded that a circular collar on the bed with  $0^\circ$  tilt is best suited for reducing local scour. Valela et al. [27] developed a new collar over

the traditional flat collar. The best collar design was achieved using OpenFOAM software. Furthermore, an iteration hybrid process was utilized to get the improved collar, and it was tested physically and observed that it performed better than the traditional collar by 11%. This paper investigates scour depth reduction around the bridge pier with and without AFC using FLOW-3D.

## 2 Governing equation

### 2.1 Large Eddy Simulation (LES)

For simulating the turbulent flow, LES is considered as the most popular technique. According to Kolmogorov’s theory of self-similarity from 1941, the geometry of the flow affects the large eddies, while the smaller scales tend to be more universal [34–37]. This characteristic allows for explicit solving of the large eddies during calculations, with the smaller eddies being implicitly accounted for by incorporating a Sub Grid-Scale (SGS) model. For incompressible flow, the filtered Navier–Stokes equation is employed as LES. This is given by the following eqs:

$$\frac{\partial \rho}{\partial t} + \frac{\partial(\rho \bar{u}_i)}{\partial x_i} = 0 \tag{1}$$

$$\frac{\partial \bar{u}_i}{\partial t} + \bar{u}_j \frac{\partial \bar{u}_i}{\partial x_j} = -\frac{1}{\rho} \frac{\partial \bar{p}}{\partial x_i} + \frac{\partial}{\partial x_j} \left( \nu \frac{\partial \bar{u}_i}{\partial x_j} \right) + \frac{1}{\rho} \frac{\partial \tau_{ij}}{\partial x_j} \tag{2}$$

where  $\rho$  is the fluid density,  $t$  is time,  $\bar{u}_i$  are filtered velocities in  $i^{\text{th}}$  direction,  $x_i$  ( $i = 1, 2 \text{ and } 3$ ) are three axes in the cartesian coordinate system,  $p$  is filtered pressure,  $\nu$  is kinematic viscosity and the term  $\frac{\partial \tau_{ij}}{\partial x_j}$  brings the nonlinearity in the system because of  $\overline{u_j \frac{\partial u_i}{\partial x_j}} \neq \bar{u}_j \frac{\partial \bar{u}_i}{\partial x_j}$  hence,

$$\tau_{ij} = \bar{u}_i \bar{u}_j - \overline{u_i u_j} \tag{3}$$

where  $\tau_{ij}$  is SGS stress and similar equations can be derived for the SGS field (i.e., the residual field) and it is calculated using Boussinesq’s hypothesis.

$$\tau_{ij} - \frac{1}{3} \tau_{kk} \delta_{ij} = -2\mu_t \bar{S}_{ij} \tag{4}$$

where,  $\tau_{kk}$  is the SGS stress turbulent kinetic energy,  $\delta_{ij}$  is filtered scale length,  $\mu_t$  is SGS turbulent viscosity and  $\bar{S}_{ij}$  is the rate of strain tensor for the resolved scale defined by

$$\bar{S}_{ij} = \frac{1}{2} \left( \frac{\partial \bar{u}_i}{\partial \bar{x}_j} + \frac{\partial \bar{u}_j}{\partial \bar{x}_i} \right) \tag{5}$$

Then filtered Navier–Stokes equation can be the following equation

$$\frac{\partial \bar{u}_i}{\partial t} + \bar{u}_j \frac{\partial \bar{u}_i}{\partial x_j} = -\frac{1}{\rho} \frac{\partial \bar{p}}{\partial x_i} + \frac{\partial}{\partial x_j} \left( [\mu + \mu_t] \frac{\partial \bar{u}_i}{\partial x_j} \right) \tag{6}$$

## 2.2 Sediment transport model

The volumetric sediment transport rate per bed width is given by van Rijn equation and is given as [38–40].

$$\Phi = \beta d_*^{-0.3} \left( \frac{\theta}{\theta_{cr}} - 1.0 \right)^{2.1} C_b \quad (7)$$

where  $\phi$  is dimensionless rate of bed-load transport,  $\beta$  is bed load coefficient,  $d_*$  is dimensionless particle size,  $\theta$  and  $\theta_{cr}$  are local and critical Shields parameters, respectively which are given by the Eqs. (8) and (9) [26, 41–43].  $C_b$  is the amount of sediment in a sample, expressed as a percentage of the total volume of the sample.

$$d_* = d_{50} \left( \frac{(G_s - 1)g}{v^2} \right)^{1/3} \quad (8)$$

$$\theta_{cr} = \frac{0.3}{1 + 1.2d_*} + 0.055(1 - e^{-0.2d_*}) \quad (9)$$

where  $G_s$  is the relative density of sediment particles,  $g$  is the gravitational acceleration constant.

## 3 Experimental and numerical setup

Experiments are conducted in a rectangular flume of length 10.3 m, width of 0.8 m and 0.5 m depth located in the Hydraulic lab in the department of civil engineering at NIT Warangal, as shown in Fig. 1. The working section of the flume is situated at a distance of 4 m from the inlet and has dimensions of 2.3 m in length, 0.8 m in width, and 0.3 m in depth. The circular pier of 5 cm diameter ( $b$ ) is considered in this study and is kept at the centre of the working section. The sediment bed is prepared with uniform sand with median size diameter ( $d_{50}$ ) of 0.32 mm with standard deviation ( $\sigma = \sqrt{d_{84}/d_{16}}$ ) 1.31 where the median particle size  $d_{84}$  and  $d_{16}$  are diameters for which 84% and 16% of the sediment particles are finer respectively [44]. The thickness of the sediment bed is 30 cm. Pier diameter ( $b$ ) is selected such that effect of sidewall and contraction effect are negligible. In channel, discharge is measured by an ultrasonic flowmeter with an accuracy of  $\pm 0.0001$  m<sup>3</sup>/s installed at the pipe inlet's exit. All the experiments are conducted with constant water depth ( $y = 10$  cm) and under clear condition, i.e.,  $V/V_c < 1$  to ensure no transport of

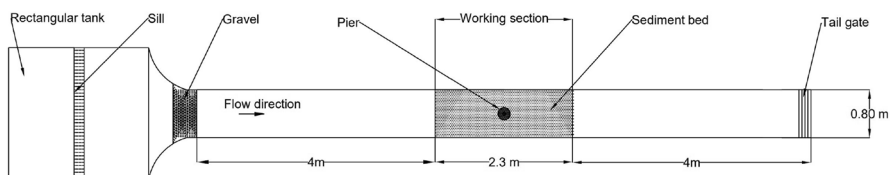


Fig. 1 Layout of the experimental setup (plan view)

sediment into the scour hole from upstream, where  $V$  and  $V_c$  are approach and critical flow velocities respectively. The study is carried out with the flow intensity ( $V/V_c$ ) of 0.95.

Figure 2a shows the simulation setup of the working section in FLOW-3D. The pier is placed at center of the working section with AFC attached to it. The AFC geometry is built in AUTOCAD and is imported to FLOW-3D. The two different collars of 4 mm thickness are used in the study with a diameter of  $d_{c1}$  (2b) and  $d_{c2}$  (3b) and a length of 4b and 6b. Figure 2b shows the description of the AFC  $d_{c1}$ . The input properties of sediment and hydraulic conditions are shown in Table 1. Simulations are carried out for six cases, as shown in Table 2.

### 3.1 Mesh sensitivity analysis

Sensitivity analysis of meshing in CFD is an important consideration to estimate scour depth. Four different mesh cell sizes are used to validate the numerical results with experimental results. A nested mesh configuration in which coarse mesh cells cover the entire geometry and finer meshing is used near the pier with AFC. The total number of mesh cells is 12,233,789 (12.234 million), with coarse cells of 2,225,664 and fine cells of 10,008,125. Table 3 shows the mesh sensitivity analysis and it is observed that decreasing the mesh cell size increases the accuracy of the results. So, the study uses coarse and fine cell sizes of 0.8 and 0.4 cm, respectively. Meshing is done using the Fractional Area-Volume Obstacle Representation (FAVOR) method for complex geometry [45]. A computer with 128 GB RAM and i-7 processor is used to simulate the scour process with the simulation running for eight to twelve days.

### 3.2 Boundary and initial conditions

The input boundary conditions used in the simulation is shown in Fig. 3b. The upstream and downstream boundary conditions are velocity ( $V$ ) and continuative ( $C$ ), respectively. Floor, lateral and free surface boundary conditions are wall ( $W$ ), wall ( $W$ ) and symmetry ( $S$ ), respectively. The initial water depth and pressure distribution used in the simulation are 0.5 m and hydrostatic pressure, respectively.

### 3.3 Validation of LES model from previous research

The experimental data of Melville and Raudkivi [16] is utilized to verify the accuracy of the LES. This same data was also utilized by Qi et al. [25] in their numerical simulation validation process. The experiments were carried out in a rectangular flume of 19 m in length, 0.456 m in width and 0.44 m in depth. A cylindrical pier of diameter 5.08 cm was used as bridge pier with uniform sediment of median size ( $d_{50}$ ) of 0.385 mm. The approach velocity and flow depth are 0.25 m/s and 15 cm, respectively. The experiment continued for several hours, and during the first 30 min, the depth of the scour hole increased rapidly, but subsequently progressed at a slower rate. The simulation has same conditions as in experimental setup. The velocity, continuity, wall, wall, and symmetry boundary conditions are applied to the upstream, downstream, floor, lateral side, and free surface, respectively. To validate the observed data of Melville and Raudkivi [16] in a simulation model, the parameters such as critical Shields number, entrainment coefficient, angle of repose, bed roughness, and bed load coefficient of 0.033, 0.018,  $32^\circ$ , 2.5, and 0.050 respectively

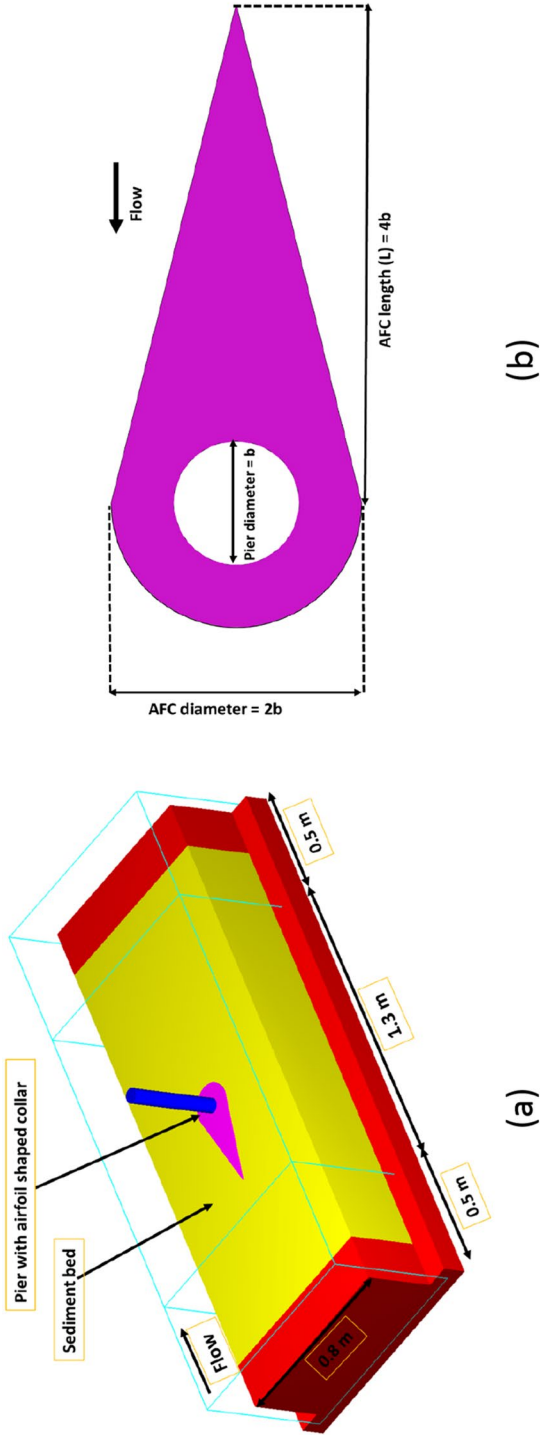


Fig. 2 **a** Simulation setup and **b** description of collar  $d_{c,1}$

**Table 1** Sediment and hydraulic conditions in the simulation setup

Median particle size, $d_{50}$ (mm)	Specific gravity of sediment, $G_s$	Critical Shields parameter, $\theta_{cr}$	Angle of repose	Bed load coefficient	Flow depth, $y$ (cm)	Critical flow velocity, $V_c$ (m/s)	Froude number, $F_r$
0.32	2.65	0.033	29°	0.045	10	0.26	0.26

are considered. The study uses nested mesh configuration of coarse and fine cell sizes of 0.8 and 0.4 cm, respectively.

## 4 Results and discussion

### 4.1 Results of LES model from previous research

The maximum scour depth around the pier is 4.073 cm and 3.89 cm from Melville and Raudkivi [16] and this simulation, respectively. The error between simulated and observed results is below 6%. Melville and Raudkivi's [16] findings indicate that the point of maximum scour depth is located at the upstream face (0°) of the pier. However, simulations suggest that it is situated within the range of 0° to 45°. The comparison between Melville and Raudkivi [16] and the simulated are shown in Fig. 4 for scour profiles. Figure 4a shows the longitudinal scour profile in which maximum scour occurs at the upstream face of the pier along the centre line of the pier, and deposition occurs behind the downstream face of the pier. As shown in Fig. 4 (b), the traverse scour hole profile is symmetrical about the pier's centre line. The findings of this study align more closely with previous research, as evidenced by the comparable maximum depth of local scour and the similar shape of the scour hole observed. From the Melville and Raudkivi [16] and simulated results, it is observed that both profiles are significantly similar. It can be concluded that LES model utilized is both reasonable and accurate, indicating its suitability for computing the utmost scouring depth surrounding the bridge pier.

### 4.2 Validation of numerical result with the present experimental result

Experiment is conducted to validate the maximum scour depth around the pier without collar, which is found to be 6.8 cm and numerical simulation for the similar condition is 6.33 cm. Thus, an error of 7% is observed, with simulation underestimating the scour depth as shown in Fig. 5. To check the accuracy of the numerical results, various statistical indices are evaluated by comparing the numerical and experimental results. The coefficient of correlation ( $R^2$ ) is calculated to assess the strength of the linear relationship between the numerical and experimental results. Additionally, the mean absolute error (MAE) is computed to determine the average magnitude of the errors in the numerical simulations [46]. The relative error percentage (REP) is utilized to quantify the discrepancy between the simulated and experimental results as a percentage of the experimental results. The root mean square error (RMSE) is also employed to measure the magnitude of the errors in the simulated results. The model's performance is evaluated using the Nash–Sutcliffe efficiency (NSE) coefficient, which compares the model's performance to the experimental results based on the mean squared error of

**Table 2** Description of simulation for six cases

Case	1	2	3	4	5	6
Location of AFC with respect to sediment bed	Pier without AFC	Pier with AFC having diameter $2b$ on sediment bed ( $d_{c1}$ )	Pier with AFC having diameter $2b$ on sediment bed in reverse to the flow direction ( $d_{c1R}$ )	Pier with AFC having diameter $2b$ at $y/2$ above the sediment bed ( $d_{c1}$ )@ $y/2$	Pier with AFC having diameter $3b$ on the sediment bed $d_{c2}$ )	Pier with AFC having diameter $3b$ at $y/2$ above the sediment bed ( $d_{c2}$ )@ $y/2$

the residuals. The value of  $R^2$ , MAE, RMSE, and NSE are evaluated using the following Eqs. (10–13), which are found to be 0.981, 3.65, 6.30 and 0.924, respectively. Overall, the results of the study indicated that the simulation has a high level of accuracy, as demonstrated by the low values of MAE, RMSE, and REP and the high value of the  $R^2$  and NSE.

$$R^2 = \left[ \frac{(N \sum M_{exp} M_{sim}) - (\sum M_{exp})(\sum M_{sim})}{\sqrt{N(\sum M_{exp}^2) - (\sum M_{exp})^2} \sqrt{N(\sum M_{sim}^2) - (\sum M_{sim})^2}} \right]^2 \tag{10}$$

$$MAE = \frac{\sum |M_{exp} - M_{sim}|}{N} \tag{11}$$

$$RMSE = \sqrt{\frac{1}{N} \sum_{i=1}^N (M_{exp} - M_{sim})^2} \tag{12}$$

$$NSE = 1 - \frac{\sum_{i=1}^N (M_{exp} - M_{sim})^2}{\sum_{i=1}^N (M_{exp} - \overline{M_{exp}})^2} \tag{13}$$

where  $M_{exp}$  and  $M_{sim}$  are experimental and simulated values,  $N$  and  $\overline{M_{exp}}$  are total no of data and average experimental values, respectively.

From the numerical simulation, 67 and 83% of equilibrium scour depths are obtained at 10 and 20% of equilibrium time. From the experimental results, the maximum scour depth location is at the pier’s upstream face ( $0^\circ$ ). But, in simulation, it is between  $0^\circ$  and  $45^\circ$ . Simulation did not estimate the location of maximum scour depth accurately because, it does not measure the velocity of turbulent pulsation. Also, the smallest mesh cell size is not capable of capturing the actual scour hole location. The second reason might be that it does not consider the sliding, rolling and jumping of sediment particles as in real-world scenarios.

### 4.3 Temporal variation of scour depth with and without AFC

The equilibrium scour depth around the pier without AFC is 6.33 cm, and with collars  $d_{c1}$ ,  $d_{c1R}$  and  $d_{c2}$ , it is 1.4, 3.5 and 0 cm, respectively when they are on the sediment bed as shown in Fig. 6. When  $d_{c1}$  and  $d_{c2}$  are at  $y/2$  above the sediment bed then, equilibrium scour depth around the pier is 5.6 and 3.6 cm, respectively. The percentage of scour reduction ( $\eta$ ) is defined as

$$\eta = \left( \frac{d - d_c}{d} \right) * 100 \quad (14)$$

where  $d$  and  $d_c$  are the maximum scour depth around the pier without and with AFC, respectively. The percentage of scour reduction using  $d_{c1}$ ,  $d_{c1R}$ ,  $d_{c2}$  on sediment bed is 77.78, 46 and 100% and for  $d_{c1}$  and  $d_{c2}$  at  $y/2$  above sediment bed is 11.12 and 42.86%. It is observed that collar  $d_{c2}$  on sediment bed is the best suited for reducing local scour around the bridge pier. The increasing order of percentages of scour reduction for collars are  $d_{c1}$  at  $y/2$  above the sediment bed,  $d_{c2}$  at  $y/2$  above the sediment bed,  $d_{c1}$  in the reverse direction to flow on the sediment bed,  $d_{c1}$  and  $d_{c2}$  on sediment bed, respectively. It is observed that the location of AFC also affects the scour depth around the pier. The collar  $d_{c1}$  is 31.78% more efficient than  $d_{c1R}$  in reducing the scour around the pier. The streamlined geometry of the AFC reduces the turbulent intensity of the flow, leading to a decrease in the strength of horseshoe and wake vortices and a reduction in the transportation of sediment particles downstream of the pier.

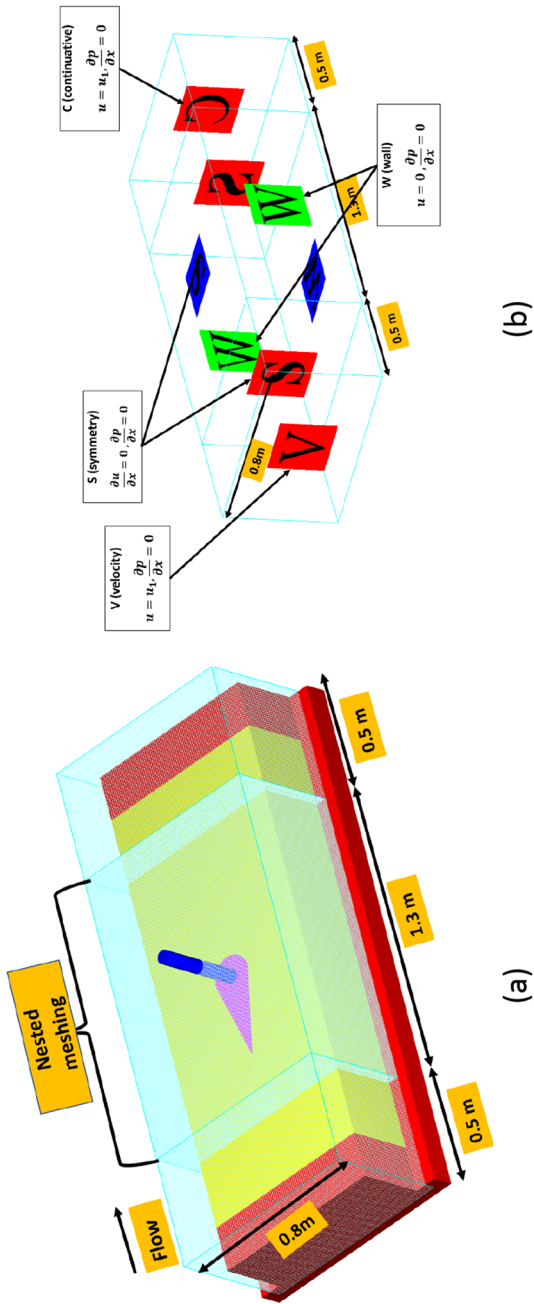
### 4.4 Morphological changes and scour depth contours

Figure 7 shows the bed morphological changes around the pier with different collar sizes placed at different elevations. These figures show equilibrium scour hole shapes, reflecting the scouring and deposition area. Using the collar, minimum scour is observed at  $d_{c2}$  on sediment bed as shown in Fig. 7 (e) and maximum scour depth at  $d_{c1}$  at  $y/2$  above the sediment bed as shown in Fig. 7d. The maximum depositions of 1.54, 1.6, 1.64, 1.55, 2.02 and 0.6 cm occurred at the distances of 33.5, 22, 23.4, 32.6, 19.2 and 31.9 cm from the centre of the pier respectively.

Scour depth contours are developed in six cases as shown in Fig. 8. Figure 8b and e shows that in the longitudinal direction, no scouring occurred around the pier. From Fig. 8c, there is no scouring in the downstream face of the pier. Also, no scour is developed around the pier with collar  $b_{c2}$  on bed level as shown in Fig. 8e. Similar pattern in contour

**Table 3** Mesh sensitivity analysis

S. N	Meshing						
	Coarse mesh cell size (cm)	Fine mesh cell size (cm)	Experimental results (cm)	FLOW-3D results (cm)	Error (%)	Estimated computational time (days)	Total no of mesh cells (million)
1	2	1	6.8	3.3	51.47	2.5	0.783
2	1	0.5	6.8	4.7	30.88	8	6.533
3	0.8	0.5	6.8	6.3	7.35	10	7.374
4	0.8	0.4	6.8	6.33	6.91	18	12.234



**Fig. 3** **a** Meshing around the geometry and **b** boundary conditions annotated

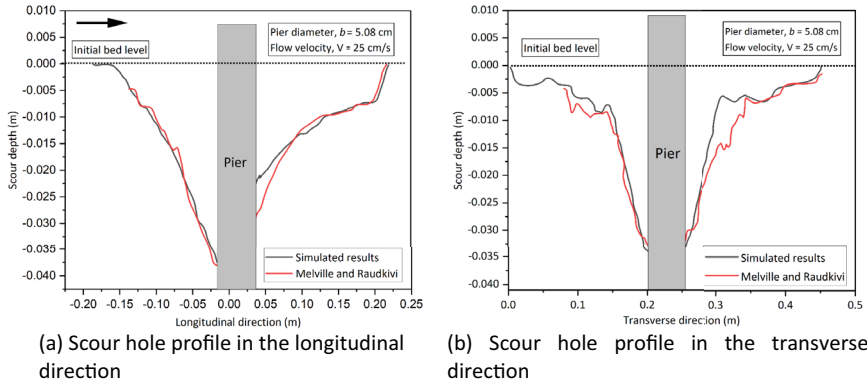
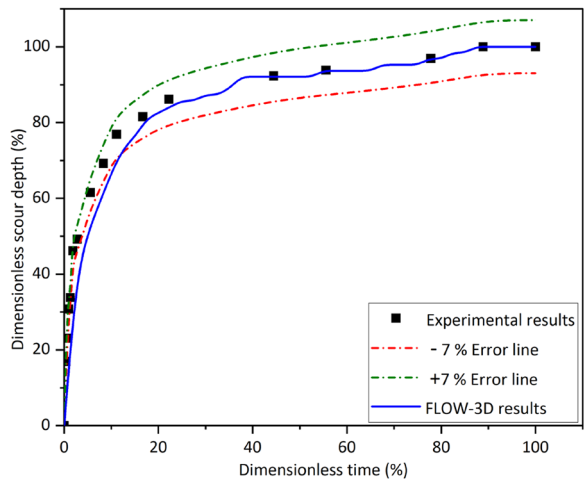


Fig. 4 Scour hole profile from Melville and Raudkivi [16] and simulated results

Fig. 5 Dimensionless scour vs time for experimental and simulation results



profiles is observed when the pier is without the collar and when the collar is placed above the sediment bed. Collars  $b_{c1}$  and  $b_{c2}$  on the sediment bed have similar profile and differ when the collar  $b_{c1}$  is placed in reverse to the flow direction.

### 4.5 Scour hole profiles

Longitudinal profiles of six cases are shown in Fig. 9. Scour occurs at the upstream face of pier and deposition at the downstream of the pier. Length of the longitudinal scour hole in six cases is 30.7, 2.17, 8.67, 26.5, 0 and 16 cm respectively. Length of transverse scour hole in six cases is 22.23, 4.1, 25.5, 22, 0 and 18 cm, respectively. Transverse profiles are symmetrical because of the circular shape of the collar in downstream face of the pier as shown in Fig. 10.

## 4.6 Plotting of the streamlines

Streamlines pattern around the pier with AFC in six cases is shown in Fig. 11. The wake regions behind the pier exhibit low flow velocity, whereas the maximum flow velocity is observed at the pier's side. When pier is attached with AFC, results in a gradual flow separation, thereby avoiding sudden flow separation. Reduction of intensity of vortices is directly related to scour reduction. Furthermore, the collar increases the number of zero-velocity streamlines around the pier, which signifies a reduction in the intensity of horseshoe and wake vortices. AFC is similar to streamline body and greatly influences the vortex system i.e., horseshoe and wake vortices. When flow bypassed the pier attached with collar, vortex system is divided into two parts; vortex above the collar and below the collar. As the local scour hole around the pier increases, the number of streamlines also increases. As a result, the vortex below the collar also increases. Number of streamlines are lesser below the collar because of the smaller scour hole.

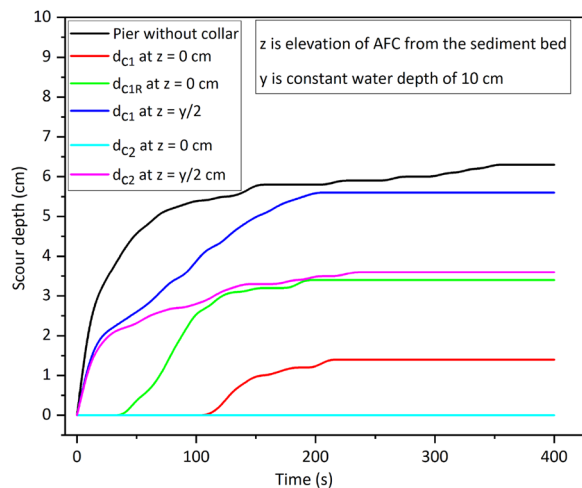
## 5 Conclusions

This study uses numerical simulation to explore the effect of the airfoil collar on local scour around the bridge pier. A total of six simulations are carried out with and without AFC. The error between the experimental and simulation result is 7% which is a good performance.

The percentage of scour reduction using  $d_{c1}$ ,  $d_{c1R}$ ,  $d_{c2}$  on sediment bed is 77.78, 46 and 100%, respectively. For  $d_{c1}$  and  $d_{c2}$  at  $y/2$  from sediment bed, it is 11.12 and 42.86%, respectively. The increasing order of percentages of scour reduction for collars are  $d_{c1}$  at  $y/2$  above the sediment bed,  $d_{c2}$  at  $y/2$  above the sediment bed,  $d_{c1}$  in reverse to flow direction on the sediment bed,  $d_{c1}$  and  $d_{c2}$  on sediment bed. The collar  $d_{c1}$  is 31.78% efficient than  $d_{c1R}$  in reducing the scour around the pier. When the collar  $d_{c1}$  and  $d_{c2}$  are placed on the sediment bed, it is observed that no scouring occurred around the upstream face of the pier. Also, with collar  $d_{c1R}$  no scouring occurred in the downstream face of the pier.

Length of the longitudinal scour hole in six cases is 30.7, 2.17, 8.67, 26.5, 0 and 16 cm, respectively. Length of the transverse scour hole in six cases is 22.23, 4.1, 25.5, 22, 0 and 18 cm, respectively. The presence of AFC significantly reduces horseshoe and wake vortices, as evidenced by the higher number of zero velocity streamlines around the pier.

**Fig. 6** Temporal variation of scour depth around the pier using AFC



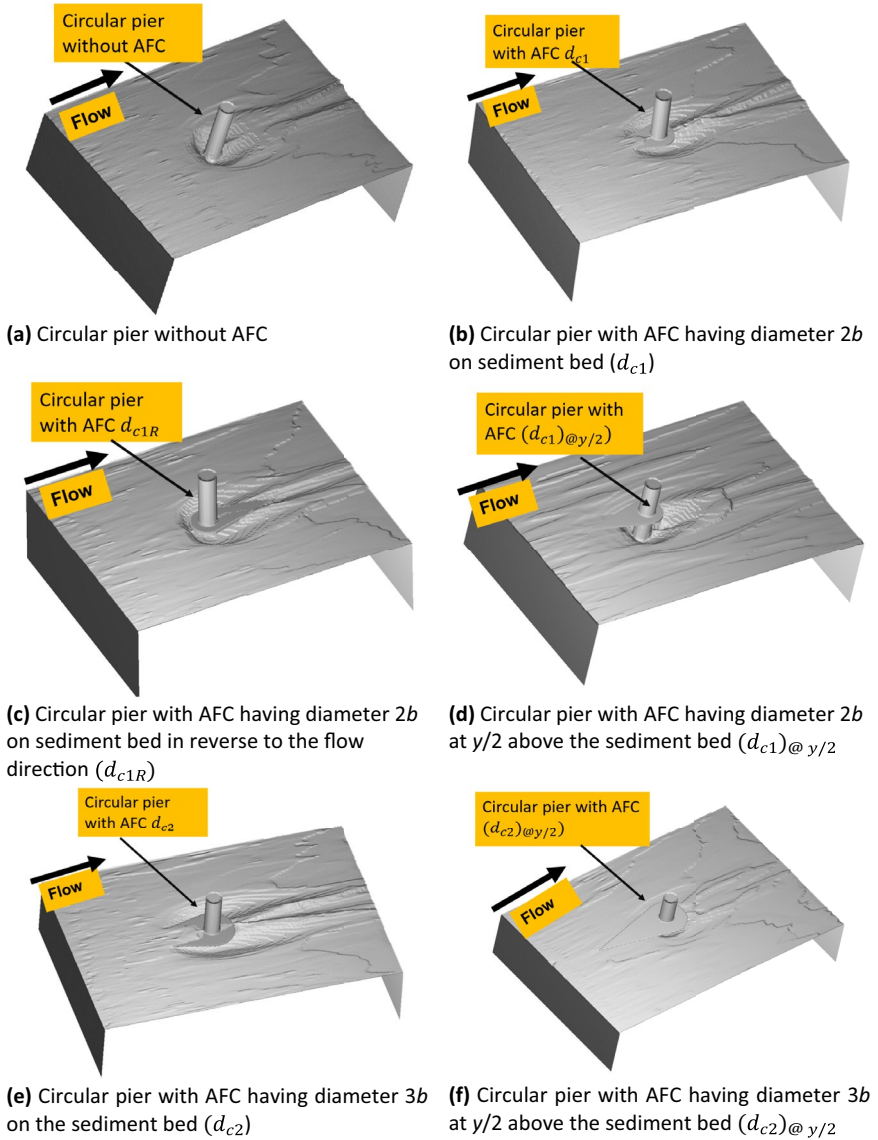


Fig. 7 Morphological changes in six different cases

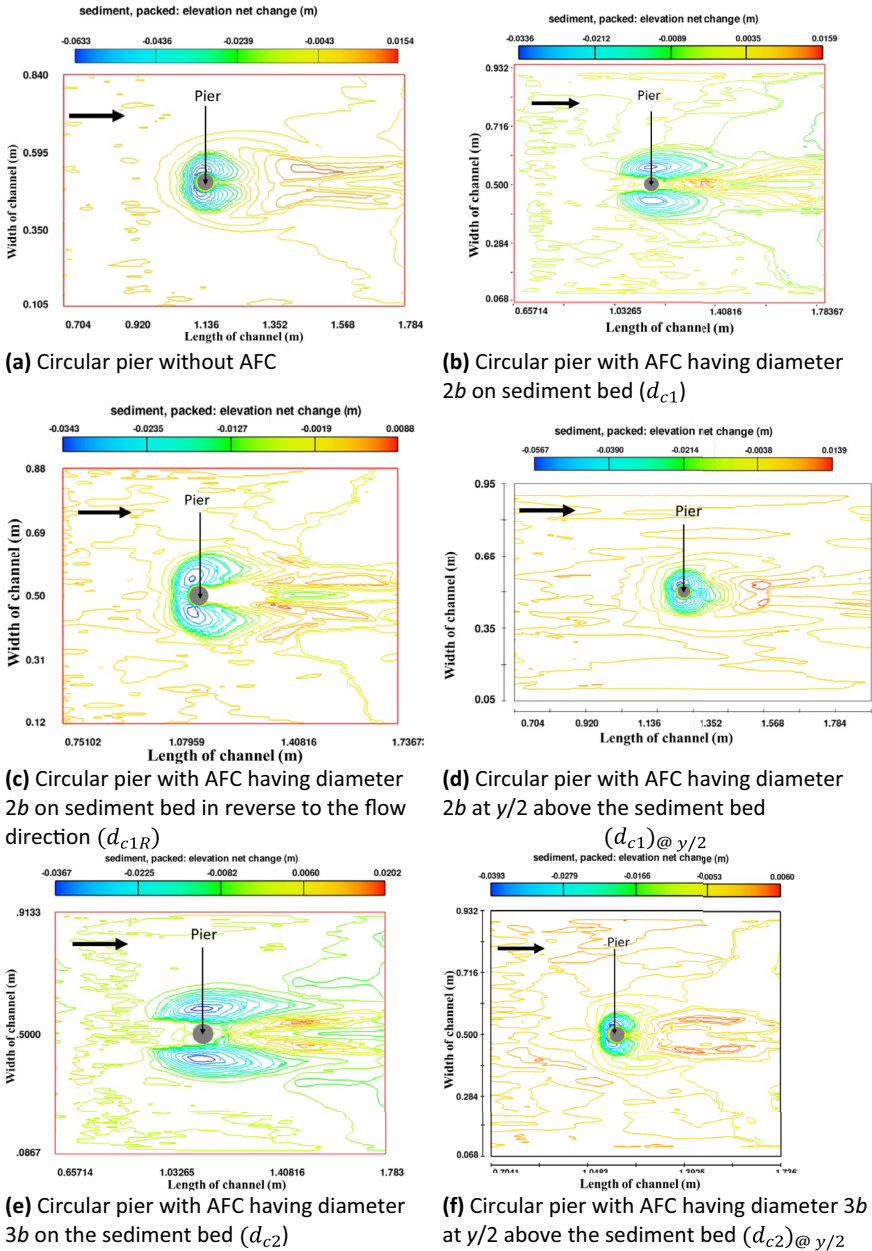


Fig. 8 Scour depth contours developed around the pier in six cases

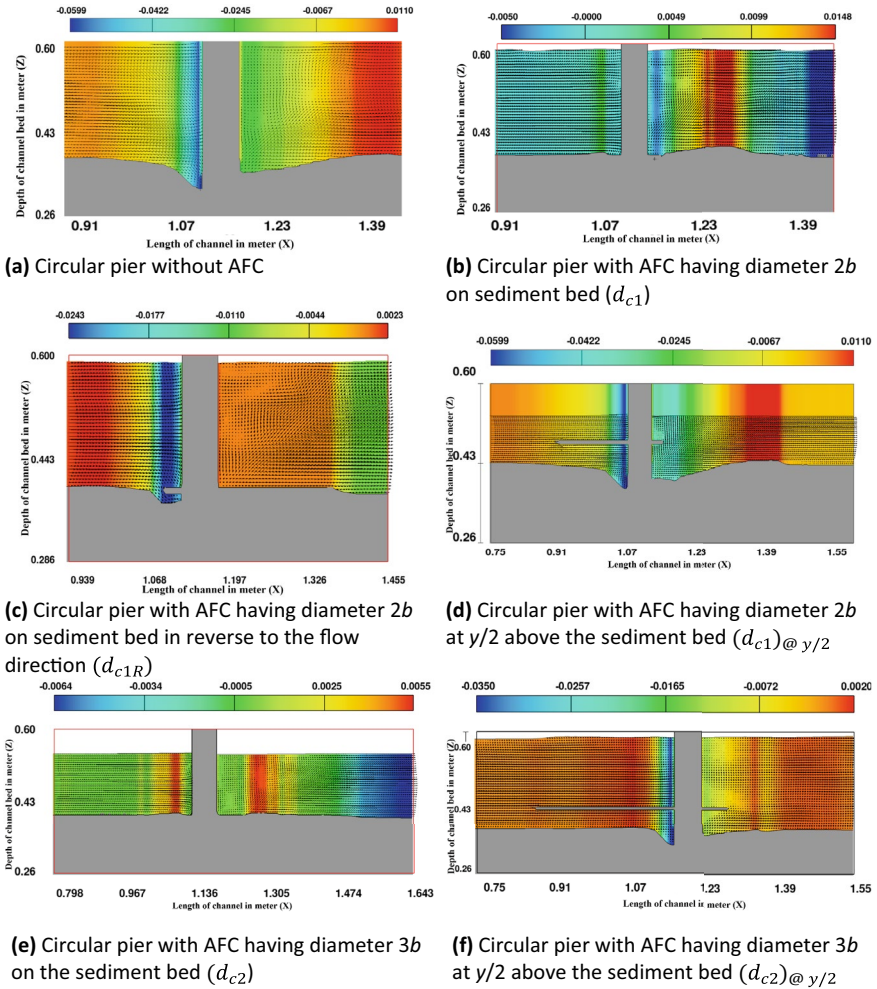


Fig. 9 Longitudinal scour hole profiles for six cases

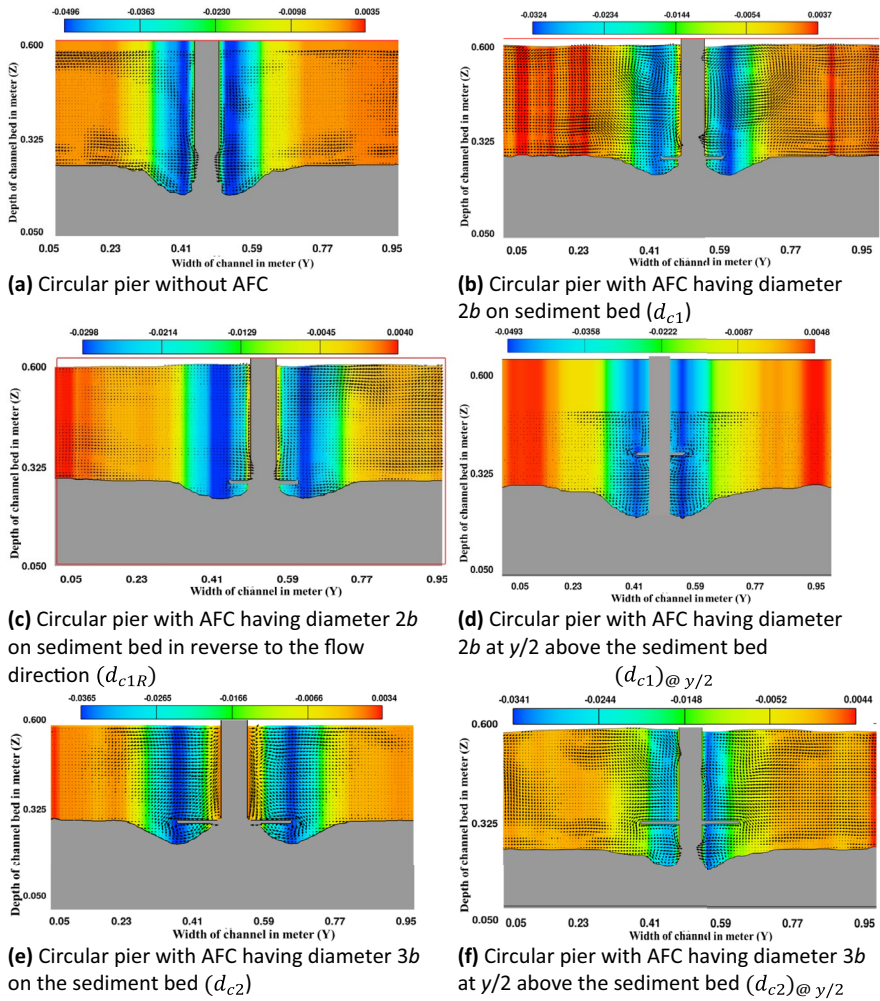
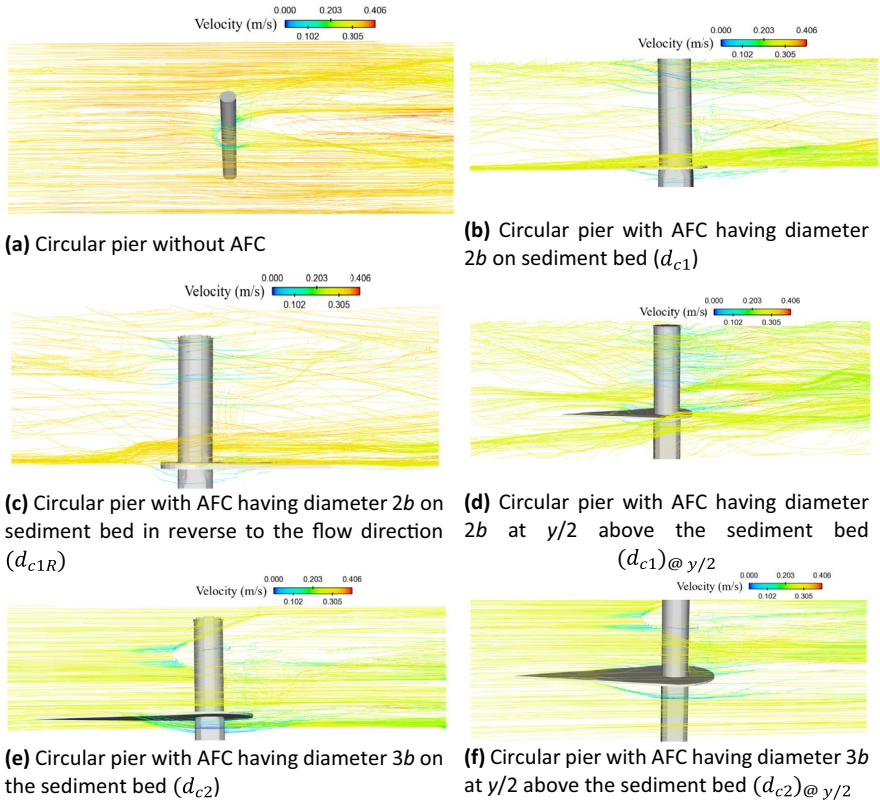


Fig. 10 Transverse scour hole profiles for six cases



**Fig. 11** Streamlines pattern around the pier with collar in six cases

**Author contributions** Conceptualization, M.P. and P.A.R.; methodology, L.K.G. and M.P.; software, L.K.G.; validation, L.K.G.; investigation, M.P. and L.K.G.; resources, M.P. and L.K.G.; data analysis, L.K.G.; writing—original draft preparation, L.K.G.; writing—review and editing, M.P., L.K.G. and P.A.R.; visualization, M.P. and P.A.R..; All authors have read and agreed to the published version of the manuscript.

**Funding** This research received no external funding.

**Declarations**

**Competing interests** The authors declare no competing interests.

**Conflict of interest** The authors declare no conflict of interest.

**References**

1. Karna N, Hari Prasad KS, Giri S, Lodhi AS (2015) Intrusion of fine sediments into river bed and its effect on river environment - A research review. *ISH J Hydraul Eng* 21:142–150. <https://doi.org/10.1080/09715010.2014.982000>

2. Gupta LK, Pandey M, Raj PA, Shukla AK (2023) Fine sediment intrusion and its consequences for river ecosystems : a review. *J Hazardous, Toxic, and Radioactive Waste* 27:1–12. [https://doi.org/10.1061/\(ASCE\)HZ.2153-5515.0000729](https://doi.org/10.1061/(ASCE)HZ.2153-5515.0000729)
3. Mathers KL, Rice SP, Wood PJ (2019) Discharge and suspended sediment time series as controls on fine sediment ingress into gravel river beds. *CATENA* 173:253–263. <https://doi.org/10.1016/j.catena.2018.10.001>
4. Deng L, Wang W, Yu Y (2016) State-of-the-art review on the causes and mechanisms of bridge collapse. *J Perform Constr Facil* 30:04015005. [https://doi.org/10.1061/\(ASCE\)cf.1943-5509.0000731](https://doi.org/10.1061/(ASCE)cf.1943-5509.0000731)
5. Melville BW (1997) Pier and abutment scour: integrated approach. *J Hydraul Eng* 123:125–136. [https://doi.org/10.1061/\(ASCE\)0733-9429\(1997\)123:2\(125\)](https://doi.org/10.1061/(ASCE)0733-9429(1997)123:2(125))
6. Kothiyari UC, Kumar A (2012) Temporal variation of scour around circular compound piers. *J Hydraul Eng* 138:945–957. [https://doi.org/10.1061/\(ASCE\)hy.1943-7900.0000593](https://doi.org/10.1061/(ASCE)hy.1943-7900.0000593)
7. Hong J-H, Chiew Y-M, Yeh P-H, Chan H-C (2017) Evolution of local pier-scour depth with dune migration in subcritical flow conditions. *J Hydraul Eng* 143:04016098. [https://doi.org/10.1061/\(ASCE\)hy.1943-7900.0001261](https://doi.org/10.1061/(ASCE)hy.1943-7900.0001261)
8. Shahriar AR, Ortiz AC, Montoya BM, Gabr MA (2021) Bridge Pier Scour: an overview of factors affecting the phenomenon and comparative evaluation of selected models. *Transp Geotech* 28:100549. <https://doi.org/10.1016/j.trgeo.2021.100549>
9. Tafarajnoruz A, Gaudio R, Calomino F (2012) Evaluation of flow-altering countermeasures against bridge pier scour. *J Hydraul Eng* 138:297–305. [https://doi.org/10.1061/\(ASCE\)hy.1943-7900.0000512](https://doi.org/10.1061/(ASCE)hy.1943-7900.0000512)
10. Pandey M, Pu JH, Pourshahbaz H, Khan MA (2022) Reduction of scour around circular piers using collars. *J Flood Risk Manag* 15:1–16. <https://doi.org/10.1111/jfr3.12812>
11. Bussi G, Francés F, Horel E et al (2014) Modelling the impact of climate change on sediment yield in a highly erodible Mediterranean catchment. *J Soils Sediments* 14:1921–1937. <https://doi.org/10.1007/s11368-014-0956-7>
12. Aly AM, Dougherty E (2021) Bridge pier geometry effects on local scour potential: a comparative study. *Ocean Eng*. <https://doi.org/10.1016/j.oceaneng.2021.109326>
13. Harrison E, Norris R, Wilkinson S (2007) The impact of fine sediment accumulation on benthic macroinvertebrates: implications for river management. Proceedings of the 5th Australian Stream Management Conference. Australian rivers: making a difference. Proc 5th Aust Stream Manag Conf Aust rivers Mak a Differ 139–144
14. Khullar NK, Kothiyari UC, Ranga Raju KG (2013) Study of deposition of fine sediment within the pores of a coarse sediment bed stream. *Int J Sediment Res* 28:210–219. [https://doi.org/10.1016/S1001-6279\(13\)60032-3](https://doi.org/10.1016/S1001-6279(13)60032-3)
15. Chiew YM, Melville BW (1987) Local scour around bridge piers Local scour around bridge piers. *J Hydraul Res* 25:15–26
16. Melville BW, Raudkivi AJ (1977) FLOW CHARACTERISTICS IN LOCAL SCOUR AT BRIDGE PIERS. *J Hydraul Res* 15:373–380. <https://doi.org/10.1080/00221687709499641>
17. Breusers HNC, Nicollet G, Shen HW (1977) Local Scour Around Cylindrical Piers. *J Hydraul Res* 15:211–252. <https://doi.org/10.1080/00221687709499645>
18. Chiew Y (1992) Scour Protection at Bridge Piers. *J Hydraul Eng* 118:1260–1269. [https://doi.org/10.1061/\(ASCE\)0733-9429\(1992\)118:9\(1260\)](https://doi.org/10.1061/(ASCE)0733-9429(1992)118:9(1260))
19. Camporeale C, Perucca E, Ridolfi L, Gurnell AM (2013) Modeling the interactions between river morphodynamics and riparian vegetation. *Rev Geophys* 51:379–414. <https://doi.org/10.1002/rog.20014>
20. Ahmed QA, Atiq M, Rehman U (2022) Effects of hooked-collar on the local scour around a lenticular bridge. *Int J Sediment Res*. <https://doi.org/10.1016/j.ijsrc.2022.07.002>
21. Mming L, Cheng WH, Qiang TG et al (2022) Investigation of local scour around two vertical piles by using numerical method. *Ocean Eng* 244:110405. <https://doi.org/10.1016/j.oceaneng.2021.110405>
22. Lagasse, P. F., Clopper, P. E., Zevenbergen, L. W., & Girard LG (2007) Countermeasures to Protect Bridge Piers from Scour. Transportation Research Board
23. Lagasse PF, Clopper PE, Pagan-Ortiz JE et al (2009) Bridge scour and stream instability countermeasures: experience, selection, and design guidance-third edition. *Hydraul Eng Circ* 2:376
24. Hong J-H, Chiew Y-M, Lu J-Y et al (2012) Houfeng bridge failure in Taiwan. *J Hydraul Eng* 138:186–198. [https://doi.org/10.1061/\(ASCE\)hy.1943-7900.0000430](https://doi.org/10.1061/(ASCE)hy.1943-7900.0000430)
25. Qi H, Tian W, Zhang H (2021) Modeling local scour around a cylindrical pier with circular collar with tilt angles (Counterclockwise around the direction of the channel cross-section) in clear-water. *Water (Switzerland)*. <https://doi.org/10.3390/w13223281>
26. Pourshahbaz H, Abbasi S, Pandey M et al (2020) Morphology and hydrodynamics numerical simulation around groynes. *ISH J Hydraul Eng* 00:1–9. <https://doi.org/10.1080/09715010.2020.1830000>

27. Valela C, Nistor I, Rennie CD et al (2021) Hybrid modeling for design of a novel bridge pier collar for reducing scour. *J Hydraul Eng*. [https://doi.org/10.1061/\(ASCE\)hy.1943-7900.0001875](https://doi.org/10.1061/(ASCE)hy.1943-7900.0001875)
28. Bhide K, Abdallah S (2022) High-order accurate numerical simulation of supersonic flow using RANS and LES guided by turbulence anisotropy. *Fluids*. <https://doi.org/10.3390/fluids7120385>
29. Kirkil G, Constantinescu G, Ettema R (2009) Detached Eddy Simulation Investigation of Turbulence at a Circular Pier with Scour Hole. *J Hydraul Eng* 135:888–901.
30. Chamani R, Rajaratnam N, Beirami MK, Sakhalkar S V (2011) Discussions and Closures Discussion of “ Turbulent Jet Energy Dissipation at Vertical Drops ” by Mohammad Closure to “ Turbulent Jet Energy Dissipation at Vertical Drops ” by Mohammad R . Chamani , Discussion of “ Energy Dissipation and Turbulent Producti. 134: 1532–1535.
31. Koken M, Constantinescu G (2008) An investigation of the flow and scour mechanisms around isolated spur dikes in a shallow open channel: 1. Conditions corresponding to the initiation of the erosion and deposition process. *Water Resour Res* 44:1–19. <https://doi.org/10.1029/2007WR006489>
32. Gupta LK, Pandey M, Raj PA, Pu JH (2023) Scour reduction around bridge pier using the airfoil-shaped collar. *Hydrology* 10:77.
33. Chen SC, Tfwala S, Wu TY et al (2018) A hooked-collar for bridge piers protection: Flow fields and scour. *Water (Switzerland)* 10:1–12. <https://doi.org/10.3390/w10091251>
34. Hinterberger C, Rodi W (2007) Three-dimensional and depth-averaged large-eddy simulations of some shallow water flows. *J Hydraul Eng* 133:857–872
35. Armenio V (2017) Large eddy simulation in hydraulic engineering: examples of laboratory-scale numerical experiments. *J Hydraul Eng* 143:1–19. [https://doi.org/10.1061/\(ASCE\)hy.1943-7900.0001357](https://doi.org/10.1061/(ASCE)hy.1943-7900.0001357)
36. Dhamankar NS, Blaisdell GA, Lyrintzis AS (2018) Overview of turbulent inflow boundary conditions for large-eddy simulations. *AIAA J* 56:1317–1334. <https://doi.org/10.2514/1.J055528>
37. Keating A, Piomelli U, Balaras E, Kaltenbach HJ (2004) A priori and a posteriori tests of inflow conditions for large-eddy simulation. *Phys Fluids* 16:4696–4712. <https://doi.org/10.1063/1.1811672>
38. van Rijn LC (1984) Sediment transport, part I: bed load transport. *J Hydraul Eng* 110:1431–1456
39. van Rijn LC (1984) Sediment transport, part II: suspended load transport. *J Hydraul Eng* 110:1613–1641
40. van Rijn LC (1984) Sediment transport, part III: bed forms and alluvial roughness. *J Hydraul Eng* 110:1733–1754
41. Ghaderi A, Abbasi S (2019) CFD simulation of local scouring around airfoil-shaped bridge piers with and without collar. *Sadhana - Acad Proc Eng Sci*. <https://doi.org/10.1007/s12046-019-1196-8>
42. Li GLL (2016) 3D numerical simulation of flow field and local scour around spur dikes. *Shuidonglixue Yanjiu yu Jinzhan Chinese J Hydrodyn Ser A* 31:372–378
43. Kuhnle RA, Alonso CV, Shields FD (2002) Local scour associated with angled spur dikes. *J Hydraul Eng* 128:1087–1093. [https://doi.org/10.1061/\(ASCE\)0733-9429\(2002\)128:12\(1087\)](https://doi.org/10.1061/(ASCE)0733-9429(2002)128:12(1087))
44. Dey S, Bose SK, Sastry GLN (1995) Clear water scour at circular piers: a model. *J Hydraul Eng* 121:869–876. [https://doi.org/10.1061/\(ASCE\)0733-9429\(1995\)121:12\(869\)](https://doi.org/10.1061/(ASCE)0733-9429(1995)121:12(869))
45. Flow Science I (2016) Flow-3d User Manual: V11.2 ; Flow Science: Santa Fe, NM, USA
46. Guguloth S, Pandey M (2023) Accuracy evaluation of scour depth equations under the submerged vertical jet. *AQUA-Water Infrastructure, Ecosyst Soc* 00:1–19. <https://doi.org/10.2166/aqua.2023.015>

**Publisher's Note** Springer Nature remains neutral with regard to jurisdictional claims in published maps and institutional affiliations.

Springer Nature or its licensor (e.g. a society or other partner) holds exclusive rights to this article under a publishing agreement with the author(s) or other rightsholder(s); author self-archiving of the accepted manuscript version of this article is solely governed by the terms of such publishing agreement and applicable law.